Kidney International, Vol. 63 (2003), pp. 2134–2143

Cell senescence in rat kidneys in vivo increases with growth and age despite lack of telomere shortening

Anette Melk, Wipawee Kittikowit, Irwindeep Sandhu, Kieran M. Halloran, Paul Grimm, Bernhard M.W. Schmidt, and Philip F. Halloran

Department of Medicine, Division of Nephrology and Immunology, University of Alberta, Edmonton, Alberta, Canada; Department of Laboratory Medicine and Pathology, University of Alberta, Edmonton, Alberta, Canada; Department of Pediatrics, University of California, San Diego, California; and Department of Medicine IV/Nephrology, University of Erlangen-Nürnberg, Germany

Cell senescence in rat kidneys in vivo increases with growth and age despite lack of telomere shortening.

Background. Somatic cells in vitro have a finite life expectancy before entering a state of senescence, but it is unclear whether this state occurs in vivo in kidney development, growth, and aging. We previously showed that human kidney cortex displays telomere shortening with age. In this study, we compared the structural and functional changes in rat kidney with age to phenomena associated with cellular senescence in vitro.

Methods. We assessed the changes in Fischer 344 rat kidneys from age 1 to 9 months to define growth and development and from age 9 to 24 months to define aging.

Results. Rat kidney telomeres were approximately 35 to 40 kb long and did not shorten significantly. Expression of mRNA for $p16^{INK4a}$, a characteristic senescence gene in vitro, was undetectable in most young rats but rose 27 fold during growth and a further 72-fold during aging. $p16^{INK4a}$ protein was localized to the nucleus and increased with age. $p16^{INK4a}$ mRNA also increased in other tissues. Lipofuscin and senescence-associated β-galactosidase increased in epithelium with growth and aging and their occurrence was significantly associated with each other. Lipofuscin was particularly found in atrophic nephrons.

Conclusion. We conclude that cell senescence occurs in both growth and aging in rat kidney and may contribute to the age-related pathology. These changes are not due to telomere shortening, but may reflect cumulative environmental stress.

Renal aging and the phenotype of age, which is termed renal senescence, are important clinical issues [1, 2]. Renal senescence is associated with many health problems, increased renal cancer, a high incidence of end stage renal disease, and poor performance of renal transplants from the elderly. Kidney aging is associated with functional and anatomic changes [3–7]. The cellular and molecular basis of renal aging remains largely unknown, but environmental stress and genomic changes such as loss of telomeres are believed to contribute [8, 9]. One possible explanation of the phenotypic changes of renal aging is that critical cells reach their finite limits and develop changes analogous to the limits reached by somatic cells in culture. Cultured mammalian somatic cells such as fibroblasts, after a finite number of population doublings, eventually reach a state in which they irreversibly cease replication and manifest abnormalities [10]. This state has been called replicative senescence for human cells and stasis for murine cells [11], but herein will be referred to as cell senescence. Mouse and human fibroblasts in vitro show major differences in how the state of senescence is reached [11]. Human cells manifest loss of telomeres, and their state of senescence can be bypassed by transfection of telomerase, which greatly extends their replicative capacity. In contrast, mouse fibroblasts show even more limited proliferative capacity in vitro, but their long telomeres are not limiting and the senescent state is produced by environmental stress ("culture shock") [11–15]. However, mouse and human cells at arrest manifest similar changes, including expression of a cell cycle regulator $p16^{INK4a}$ and organelle changes such as senescence-associated β-galactosidase (SA-β-GAL) and lipofuscin [16–19]. Cell senescence could also occur during renal development and growth as well as during aging.

Aging events in rat kidneys are of interest in themselves and for comparison to the processes of human kidney senescence. There is a wide variability in the effects of aging on the rat kidney. In particular, strains differ in the development of proteinuria that is associated with glomerular changes, typically focal and segmental sclerosis [20], and the environment influences the phenotype within strains. Rat kidneys, unlike human kidneys, manifest no

Key words: aging, senescence, telomere, $p16^{INK4a}$, lipofuscin, senescence-associated β-galactosidase, Fischer 344.

Received for publication September 16, 2002
and in revised form December 12, 2002
Accepted for publication February 4, 2003

loss of renal mass and little or no loss of function with age unless they have concomitant kidney disease [21, 22].

In this study we explored whether characteristic features of senescence in cultured cells develop in the rat kidney with development and aging. Senescent cells in vitro are resistant to apoptosis, and could persist in their abnormal state and thus contribute to pathology in complex tissues and organs, interfering with organ homeostasis. Our purpose was to seek evidence for or against the concept that cell senescence as defined in culture is actually a phenomenon in vivo, and that it may contribute to the phenotype of renal aging. This in turn would assist in generating testable models of renal aging.

METHODS

Kidneys

Rat samples were derived from 32 Fischer 344 rats of three age groups (1 month, $N = 11$; 9 months, $N = 10$; and 24 months, $N = 11$). One-month-old rats were derived from the University of Alberta animal colony and 9- and 24-month-old rats from the NIA colony were purchased from Harlan (Indianapolis, IN, USA) (9- and 24-month-old age group). All animals were housed barrier maintained and specific pathogen free. The animals were killed within 1 week after arrival in our colony.

Rats were anesthetized and blood was drawn for measurement of serum creatinine, urea, and electrolytes. Then a midline incision was performed and kidneys, spleen, and heart were quickly removed. Brains were harvested last. All tissue samples were immediately snap-frozen in liquid nitrogen and stored at –70°C. In addition, tissue was embedded in 22-oxacalcitriol (OCT) for frozen sections and fixed with paraformaldehyde for paraffin-embedded sections. All experiments were performed according to the University of Alberta Animal Policy and Welfare Committee's animal care protocols.

Pathology and lipofuscin assessment

Paraffin wax sections were cut at 2 μm and stained with hematoxylin and eosin, periodic acid-Schiff and Masson trichrome for histopathologic assessment by one pathologist (W.K.). Two independent observers performed lipofuscin counts using high power field. Both assessments were done blinded.

Sirius Red staining

Unstained paraffin embedded sections were baked at 60°C for one hour. Slides were soaked in xylene for 24 hours followed by acetone for 24 hours to reduce paraffin contamination. Then slides were taken through xylene and graded ethanols into distilled water and stained overnight in saturated picric acid with 0.1% Sirius Red F3BA (Aldrich Chemicals, Oakville, Ontario, Canada). Slides were washed in hydrochloric acid (0.01 N) and rapidly dehydrated and mounted. Sirius Red staining was only performed on a subgroup of 12 rats (1 month, $N = 5$; 9 months, $N = 2$; and 24 months, $N = 5$).

Image analysis was performed by a technician blinded to the source of the sample. The slides were examined with a Nikon E600 microscope, and a Hitachi analog 3 charged coupling device (CCD) camera was used to capture gray scale 256 bit images that were archived as tagged-image file format (TIFF) files. A background image was initially obtained and background correction was performed in real time while the images were being acquired using the ×40 objective. Images of the kidney cortex were obtained in a serpentine fashion starting at one end of the tissue and working toward the other. Large glomeruli, vessels larger than the size of adjacent tubules and the medulla were not included in the image acquisition. Image analysis was performed using an automated macro (available from P.G.) specially written for the software package NIH Image. Automated analysis of the images was performed with operator supervision. Data is expressed as cortical fractional interstitial fibrosis volume (V_{IntFib}), a value of 1 would reflect 100% fibrosis.

Terminal restriction fragments (TRF)

To obtain high molecular weight DNA without degradation, the tissue was disrupted by freeze grinding. DNA was then isolated by proteinase K digestion and phenol/chloroform extraction. Concentration was measured at optical density $(OD)_{260}$. DNA samples were digested with the restriction enzymes Hinf I and Rsa I (Boehringer Mannheim, Germany) to produce terminal restriction fragments (TRFs). Each digested sample (1.5 μg) was resolved on a 1.0% agarose gel by pulse field gel electrophoresis (buffer temperature 14°C, voltage gradient 6.0 V/cm, switching interval 1 to 30 seconds, 12 hours). Gel was probed directly as described previously [23] with minor modifications [24]. Hybridization was done at 42°C overnight with a 5′ end-labeled ^{32}P-$(TTAGGG)_5$ oligonucleotide telomere probe in a buffer containing 6 × standard sodium citrate (SSC), 5 × Denhardt's solution, 50 mmol/L NaH_2PO_4 (pH 7.4), 0.1 mg/mL salmon sperm DNA, 0.1% sodium dodecyl sulfate (SDS). Following stringency washes at reverse transcription (RT) in 0.2 × SSC, 0.1% SDS, the autoradiography signal was digitized in a phosphoimage scanner (Fuji) using ImageGauge Software. All lanes were subdivided into intervals of 1 mm. The mean size of the TRFs was estimated using the formula $\Sigma(Odi \times Li)/\Sigma(ODi)$, where ODi is the density reading from interval i and Li is the size in kilobase pairs of the interval relative to the markers [25]. Mean TRF length was determined on the basis of the intensity of the signal, where the intervals averaged were those intervals, which were higher than 1% of the total signal in that lane.

Real-time reverse transcription-polymerase chain reaction (RT-PCR)

Total RNA was extracted from tissue samples according to a modification of the method described by Chirgwin et al [26]. Tissues were homogenized with a polytron in 4 mol/L guanidinium isothiocyanate, and the RNA was pelleted through a 5.7 mol/L $CsCl_2$ cushion. RNA was isolated by phenol/chloroform extraction. Concentrations were determined by absorbance at 260 nm. Transcription into cDNA was done using Moloney murine leukemia virus (MMLV) reverse transcriptase and random primers (Life Technologies, Burlington, Ontario, Canada). The principle of real-time quantitative PCR has been described by Heid et al [27]. cDNA (0.75 μL) was amplified in an ABI PRISM 7700 Sequence Detector (Applied Biosystems, Foster City, CA, USA). All samples were done in duplicates. Sequence specific primers and probe for $p16^{INK4a}$ (forward primer 5′-ACG AGG TGC GGG CAC TG-3′; reverse primer 5′-TTG ACG TTG CCC ATC ATC ATC-3′; probe 5′-FAM-CCG AAC ACT TTC GGT CGT ACC CCG ATA-TAMRA-3′) and transforming growth factor-β1 (TGF-β1) (forward primer 5′-GGC TAC CAT GCC AAC TTC TGT CT-3′; reverse primer 5′-CCG GGT TGT GTT GGT TGT AGA-3′; probe 5′-FAM-CAC ACA GTA CAG CAA GGT CCT TGC CCT-TAMRA-3′) were designed using Primer Express Software (Applied Biosystems). Predeveloped assay reagents for 18S ribosomal RNA (18S RNA) were purchased (Applied Biosystems). The number of PCR cycles that are needed to reach the fluorescence threshold is called threshold cycle (Ct). The Ct value for each sample is proportional to the log of the initial amount of input cDNA. After calculation of the mean Ct value for the duplicates, the Ct values for all samples were normalized to 18S RNA by subtraction (Ct for $p16^{INK4a}$ minus Ct for 18S RNA), called ΔCt. Relative quantification of gene expression was calculated as $2^{-\Delta Ct}$. A mixture of equal amounts of different rat spleen cDNA was used as an internal control and was run with each experiment. The mean ΔCt value for this sample was 21.7 and the variation coefficient for all experiments was 2.01%.

Immunohistochemistry for $p16^{INK4a}$

Immunoperoxidase staining for $p16^{INK4a}$ was performed using 2 μm sections of paraffin-embedded tissue. Briefly, sections were deparaffinized and hydrated. The sections were immersed in 3% H_2O_2 methanol to inactivate endogenous peroxidase. Slides were blocked with 20% normal goat serum. Tissue sections were then incubated for 1 hour at RT with the primary antibody (mouse monoclonal antibody, Clone F-12, Santa Cruz Biotechnolgies, Santa Cruz, CA, USA) and rinsed with phosphate-buffered slaline (PBS). Following 30 minutes of incubation with the Envision monoclonal system (Dako, Mississauga, Ontario, Canada), sections were washed again in PBS. Visualization was performed using the diaminobenzidine (DAB) substrate kit (Dako, Ontario). The slides were counterstained with hematoxylin and mounted. Analysis was done by counting 5 high power field by a blinded observer. Percentage of positive nuclei was assessed for tubules, glomeruli, and interstitium.

Western blot analysis

Tissue was homogenized in radioimmunoprecipitation assay (RIPA) buffer containing the protease inhibitors phenylmethylsulfonylfluoride (100 μg/mL), aprotinin (100 μg/mL), and sodium orthovanadate (1 mmol/L). Homogenates were centrifuged and supernatants were snap-frozen and stored at –80°C. Protein concentrations were determined using the BioRad Lowry protein assay (Bio-Rad Labs, Hercules, CA, USA). Samples (50 μg) were loaded and proteins were separated by 11.5% sodium dodecyl sulfate polyacrylamide gel electrophoresis (SDS-PAGE) followed by electrophoretic transfer to a nitrocellulose membrane. Retinoblastoma was detected using a rabbit polyclonal antibody against total retinoblastoma (C-15, Santa Cruz Biotechnology) that showed two separate bands for phosphorylated and hypophosphorylated retinoblastoma. This was followed by peroxidase-conjugated goat antirabbit immunoglobulin G (IgG) (Jackson Immuno Research Laboratories, West Grove, PA, USA) and enhanced chemiluminescence (SuperSignal®, Pierce, IL, USA).

Senescence-associated (SA) β-galactosidase (β-GAL) staining

Frozen sections were cut at 4 μm and kept at −20°C until further processed. Staining was done according to Dimri et al [28], including modifications by Chkhotua et al [29]. Briefly, slides were brought to RT and fixed with 2% formaldehyde/0.2% glutaraldehyde in PBS. Slides were then incubated for 14 hours at 37°C in a humidified chamber with SA-β-gal staining solution [2 mg/mL × gal in dimethylformamide, 40 m mol/L citric acid/sodium phosphate (dibasic), pH 6, 5 mmol/L potassium ferrocyanide, 5 mmol/L potassium ferricyanide, 150 mmol/L sodium chloride, and 20 mmol/L magnesium chloride]. Controls were stained for lysosomal β-gal using the same SA-β-gal staining solution adjusted to pH 4. Following staining, slides were counterstained with eosin, dehydrated, and mounted.

Quantification of the SA-β-GAL staining was accomplished by Image-Pro Plus Software. A set of slides without counterstain was produced and photographed. The image was opened in Image-Pro Plus and staining density for the whole section was calculated. The mean staining density of two independent experiments was taken for further calculations and statistical analysis.

Table 1. Kidney function and weight

Groups	M ± SD 1 month	9 months	24 months
Creatinine *μmol/L*	20.4 ± 6.2	42.2 ± 10.6[a]	58.0 ± 16.9
Urea *mmol/L*	7.5 ± 1.2	8.6 ± 0.9	6.6 ± 1.1
Sodium *mmol/L*	124.6 ± 9.8	142.2 ± 13.3	134.3 ± 11.2
Chloride *mmol/L*	81.2 ± 7.1	92.8 ± 8.9	92.0 ± 8.9
Kidney weight *mg*	723 ± 70	1157 ± 107[a]	1403 ± 141[b]
Body weight *g*	152 ± 21	409 ± 54[a]	419 ± 49
Kidney/body weight ratio [10^3]	4.9 ± 0.8	2.9 ± 0.4[a]	3.4 ± 0.4[b]

[a] 1-month-old and 9-month-old group differ $P < 0.05$
[b] 9-month-old and 24-month-old group differ $P < 0.05$

Table 2. Pathology of rat kidney

Groups	M ± SD 1 month $N = 6$	9 months $N = 6$	24 months $N = 7$
Glomeruli number per section	213 ± 15.6	214 ± 23.7	254 ± 20.1[b]
Total sclerotic glomeruli %	0	0.2 ± 0.4	2.4 ± 0.9[b]
Partial sclerotic glomeruli %	0	0.1 ± 0.2	2.0 ± 2.2[b]
Glomerulitis (0–3)	0	0	0
Glomerulopathy (0–3)	0	0	0
Fusion to Bowman's capsula %	0	0	0.4 ± 0.8
Widened Bowman's space %	0	0.6 ± 0.5[a]	2.6 ± 1.9
Epithelial proliferation %	0	0	0.1 ± 0.1
Hyaline droplets %	0	0	0.5 ± 0.5[b]
Hyaline arteriole %	0	0	0.4 ± 0.4
Casts in cortex *number*	0	1.7 ± 1.4[a]	14.9 ± 11.4[b]
Casts in medulla[c]	0	0.8 ± 0.4[a]	1.6 ± 0.8
Tubular atrophy[d]	0	0.7 ± 0.8	8.0 ± 9.0[b]
Dilated tubules[d]	0	0.2 ± 0.4	3.7 ± 5.6[b]
Mononuclear infiltrate[e]	0	2.2 ± 1.9[a]	6.0 ± 6.0
Arteriolar hyaline thickening	0	0	0.6 ± 0.8
Vascular fibrous intimal thickening	0	0	0
Cells per tubular cross-section *number*	4.5 ± 0.3	4.1 ± 0.8	3.5 ± 0.4

[a] 1-month-old and 9-month-old group differ $P < 0.05$
[b] 9-month-old and 24-month-old group differ $P < 0.05$
[c] Number of cross-sections that show casts in medulla: 1 = <50 cross-sections, 2 = 50–100 cross-sections, 3 = >100 cross-sections
[d] Number of groups per kidney section that showed tubular atrophy or dilated tubules
[e] Number of areas that showed mononuclear infiltrate

Terminal deoxnucleotidyl transferase-mediated uridine triphosphate (UTP) nick end labeling (TUNEL)

Paraffin-embedded sections were deparaffinized and hydrated. The sections were immersed in 1% H_2O_2 to inactivate endogenous peroxidase. The sections were treated with proteinase K (20 μg/mL in PBS) for 10 min at RT and rinsed in PBS. Sections were incubated with terminal deoxnucleotidyl transferase (TDT) buffer (30 mmol/L Tris-HCl, pH 7.2, 1 mmol/L $CoCl_2$, and 140 mmol/L sodium cacodylate) for 30 minutes at RT. The TDT buffer was then replaced with TDT buffer containing 0.025 nmol/μL biotin-16-dUTP (Roche, Laval, Quebec, Canada) and 0.25 U/μl TDT (Roche, Laval) and incubated for 1 hour at 37°C in a humidified chamber. Slides were rinsed in PBS. Nonspecific staining was blocked by immersing the slides in 2% bovine serum albumin (BSA) in PBS. The slides were then incubated with the avidin-biotin complex (Vector Laboratories, Burlingame, CA, USA) for 30 minutes. The reaction was visualized using the DAB substrate kit (Vector Laboratories). The slides were counterstained with alcian blue, dehydrated, and mounted. For negative controls TDT was omitted. Kidney sections treated with 1000 ng/mL DNAase I (Sigma Chemical Co., St. Louis, MO, USA) were used as positive controls. Analysis was done by counting all positive nuclei per kidney section.

Statistical analysis

Data analyses were performed using SPSS (Version 11.0). Means among three groups of rats were compared using Kruskal-Wallis nonparametric tests, and Mann-Whitney tests with Bonferroni correction were used for multiple pair-wise comparisons. The Fisher exact test was used to test for differences in proportions, 1-month-old with 9-month-old, 9-month-old with 24-month-old rats.

RESULTS

Renal changes with growth and aging

Because environment, subline genetic differences [30, 31], and specific renal diseases can alter the phenotype of growth and aging in kidney [20], it was essential that we characterize the extent of the previously reported changes [20, 30–33] at each age in our rats to permit correlation with our indicators of cellular senescence. We arbitrarily termed the 1 to 9 months interval "growth" and the 9 to 24 months interval "aging." Creatinine increased significantly during growth (9 months versus 1 month) but not during aging (24 months versus 9 months); urea and electrolytes showed no changes (Table 1). We confirmed that our rats displayed this pattern. Both kidney and body weight from age 1 month to age 9 months increased by 60% and 169%, respectively. Kidney weight increased by a further 21% from 9-month-old to 24-month-old rats, but body weight did not change. The kidney-to-body-weight ratio decreased during growth and increased during aging. The protein/DNA ratio was stable for all three ages (15.2 ± 2.0 in 1-month-old vs. 15.3 ± 1.5 in 24-month-old rats).

We evaluated the histologic changes of growth and aging using a pathology scoring system incorporating features of the Banff classification for transplant pathology [34] and previous reports [20] (Table 2). None of the

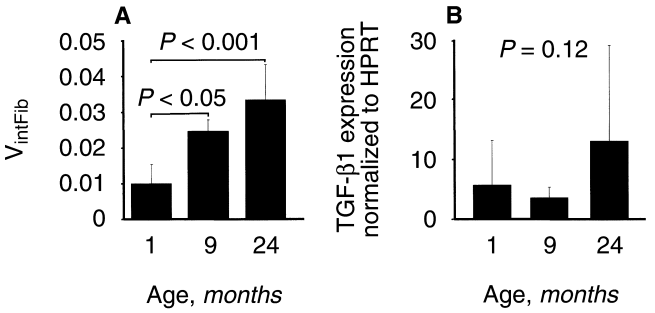

Fig. 1. Effects in three different age groups. (*A*) Fraction of cortical interstitial fibrosis in rat kidneys of three different age groups. Interstitial fibrosis increased significantly with growth, the further increase with age was not statistically significant. (*B*) Transforming growth factor-β1 (TGF-β1) mRNA expression was highly variable in young and old rats. The increase with age was not statistically significant.

1-month-old rats had features suggesting renal diseases beyond the changes of aging. By 9 months the percentage of glomeruli with widened Bowman's space and the number of casts in cortex and medulla increased, and occasional foci of mononuclear infiltrate appeared. Some rats at 9 months manifested occasional totally sclerotic (two of six) or partially (segmental) sclerotic glomeruli (one of six), tubular atrophy (three of six), and dilated tubules (one of six). By 24 months of age, all kidneys showed histologic features of aging, including total and partial (segmental) sclerosis (although only 4.4% of glomeruli were affected), hyaline droplets, tubular atrophy, interstitial fibrosis, and arteriolar hyalinosis. No rats showed arterial fibrous intimal thickening. The number of cells per tubular cross-section did not change with age.

Cortical fibrosis was quantitated by Sirius Red staining (Fig. 1A) and increased significantly with growth (V_{intFib} 0.01 ± 0.005 at 1 month vs. 0.024 ± 0.003 at 9 months; $P < 0.05$). The further increase with aging (V_{intFib} 0.033 ± 0.010 at 24 months) did not reach statistical significance. Because of the increase in fibrosis, we measured the amount of TGF-β1 mRNA (Fig. 1B). TGF-β1 expression was highest in the 24-month-old rats (13 ± 16.1) but the differences between age groups were not statistically significant.

Mean TRF length in rat kidney samples

Figure 2A shows a typical TRF length gel obtained by pulse-field gel electrophoresis. The mean ± SD for mean TRF length (kb) was 38.5 ± 1.0 for 1-month-old rats, 40.6 ± 4.8 for 9-month-old rats, and 35.1 ± 6.0 for 24-month-old rat kidneys (Fig. 2B). There was no significant change in TRF length with growth or aging ($P = 0.49$). The mean TRF length in rat samples was above 30 kb, similar to what has been shown for *Mus musculus* strains [35] and much longer than in human kidney (about 12 Kb) [36].

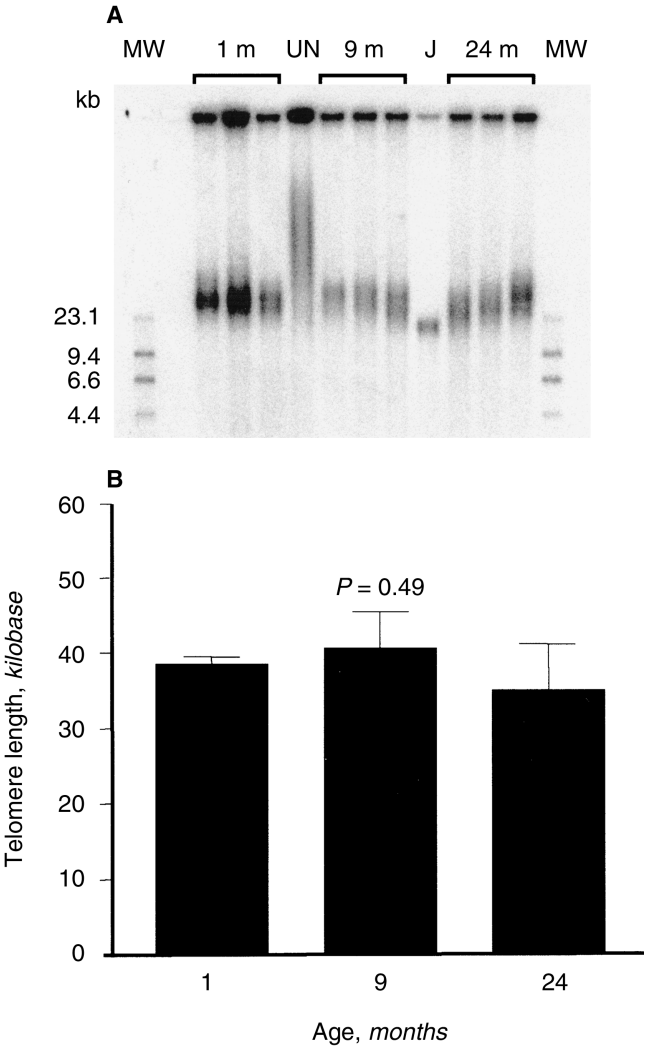

Fig. 2. Mean telomere restriction fragment (TRF) length in rat kidneys of three different age groups. (*A*) Representative TRF gel. (*B*) Mean TRF length ± SD of mean TRF length for the three different age groups. High-molecular-weight DNA was isolated, resolved by pulse-field gel electrophoresis. Hybridization with a telomere specific ^{32}P-labeled oligonucleotide was performed and mean TRF length was calculated based on the signal intensity for each lane. Size (kb) is indicated. Abbreviations are: MW, molecular weight marker; J, Jurkat cell line; UN, undigested DNA sample not digested with HinfI and Rsa I. Kruskal-Wallis test was performed for the comparison of all three groups.

$p16^{INK4a}$ mRNA expression in rat kidney, spleen, brain, and heart samples

$p16^{INK4a}$ mRNA was absent in most 1-month-old kidneys but increased 27-fold with growth and a further 72-fold with aging (Fig. 3A). The $p16^{INK4a}$ mRNA levels were undetectable in 10 out of 11 samples in 1-month-old rats and very low (1.75×10^{-9}) in the remaining one rat. Nine-month-old rats had detectable levels in all 10 animals. Highest levels were found in the group of 24-month-old rats. Mean values (±SD) for $p16^{INK4a}$ expression normalized to 18S RNA in kidney were 1.6×10^{-10} ($\pm 5.29 \times 10^{-10}$) for 1-month-old rats, 43.8×10^{-10} ($\pm 29.2 \times 10^{-10}$)

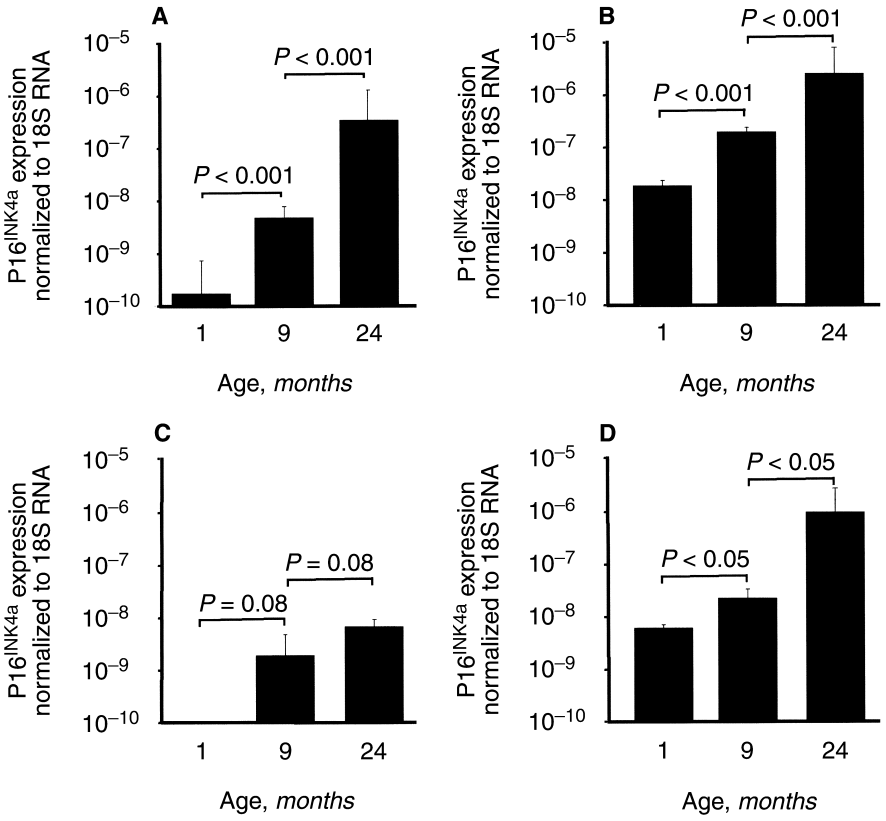

Fig. 3. $p16^{INK4a}$ mRNA expression in different rat tissues. Kidney (*A*), spleen (*B*), brain *(C)*, and heart *(D)* in three different age groups. RNA was isolated and reverse transcribed. Quantitative RT-PCR was performed using sequence-specific primer and probe for $p16^{INK4a}$ on an ABI 7700 Sequence Detection System. All values were normalized to 18S RNA.

for 9-month-old rats, and 3160×10^{-10} ($\pm 8850 \times 10^{-10}$) for 24-month-old rats. The latter group showed considerable variability in $p16^{INK4a}$ levels.

Increases in $p16^{INK4a}$ were seen for three other tissues investigated (Fig. 3) (spleen, $P < 0.001$; brain, $P < 0.05$; heart, $P < 0.05$). Interestingly, $p16^{INK4a}$ was expressed in both spleen and heart even in the 1-month-old group, whereas $p16^{INK4a}$ was not detected in any of the brain tissues for the 1-month-old rats. This was the case for most of the kidneys, but the brain showed no significant increase between 9-month-old and 24-month-old rats.

$P16^{INK4a}$ protein expression in rat kidneys

We were able to corroborate the mRNA results by immunoperoxidase staining for $p16^{INK4a}$. Representative tubular sections are shown in Figure 4. Young rat kidneys, which lacked or had very low $p16^{INK4a}$ levels showed no or occasional staining of single nuclei (mean of positive nuclei in tubules 4%; in glomeruli 4%; and in interstitium 1%). The increase with aging was highly significant for all investigated compartments. The mean of positive nuclei in 9-month-old versus 24 month-old-rats was 5% versus 46% in tubules ($P < 0.001$), 6% versus 38% in glomeruli ($P < 0.001$), and 1% versus 18% in interstitium ($P < 0.0001$). Very rarely single lymphocytes within a mononuclear infiltration stained.

By Western blot, we did not find any differences in the amount of retinoblastoma, a downstream target of $p16^{INK4a}$, between young and old rats.

SA-β-GAL

SA-β-GAL was described in senescent human fibroblast cultures [28], but not in quiescent or terminally differentiated cells, and in vivo in skin cells from old humans. SA-β-GAL has been recommended as an indicator of cell senescence in vitro [37] and in vivo [38, 39]. We assessed SA-β-GAL staining for rat specimens of different ages (for representative pictures, see Fig. 5). SA-β-GAL staining was found only in tubular cells, not in glomeruli or vessels. As can be seen in Figure 5C, a patchy pattern was observed in 24-month-old rats, suggesting those SA-β-GAL stained tubules belonged to the same nephron. SA-β-GAL staining was quantitated by a photo imaging technique for which a whole cross-section of the kidney was photographed. Mean staining densities (arbitrary units) were 0.003 ($\pm$ 0.002) for 1-month-old rats, 0.008 ($\pm$ 0.003) for 9-month-old rats, and 0.020 ($\pm$ 0.007) for 24-month-old rats ($P < 0.005$). Thus SA-β-GAL increased during growth but further increased during aging.

TUNEL

To assess the amount of apoptotic cells TUNEL staining was performed. Apoptotic cells were overall rare, but increased continuously with age. Young rats had an average of one positive nucleus per kidney cross-section, 9-month-old rats had six positive nuclei, and in 24-

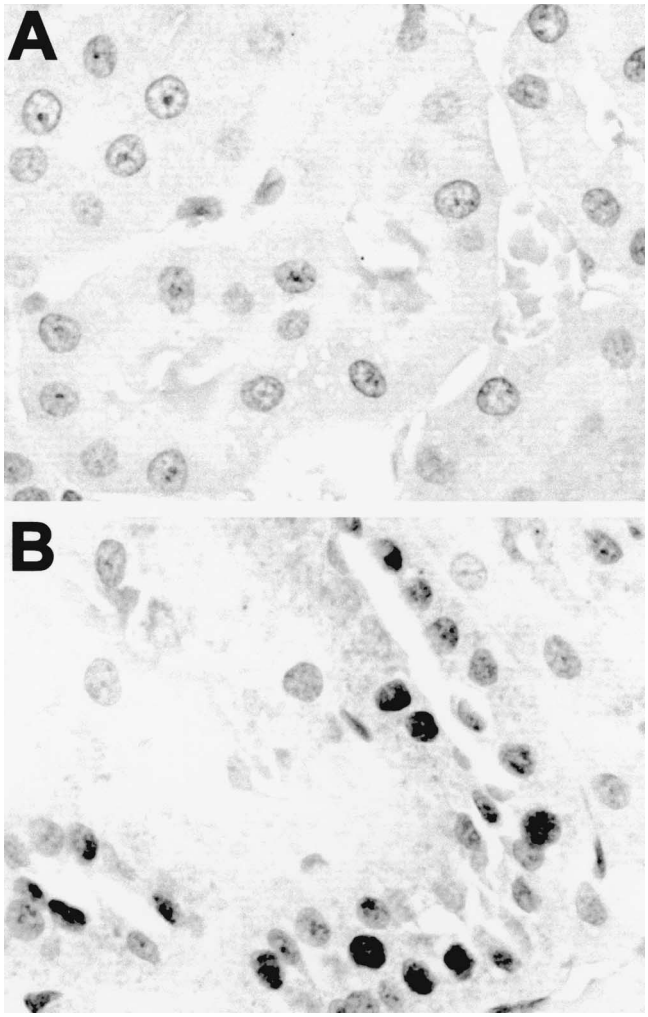

Fig. 4. Representative p16^{INK4a} staining in rat kidney tubular sections from a (*A*) 1-month-old, and (*B*) 24-month-old rat. Immunoperoxidase staining was performed on paraffin sections with a monoclonal antibody against p16^{INK4a} and hematoxylin counterstain. Nuclear p16^{INK4a} staining was not or very rarely found in young, but was present in all old rat kidneys.

month-old rats we found 12 positive nuclei. Positive nuclei were almost always found in tubules, interstitial cells showed some positive nuclei, and only one old rat had a positive nucleus in its glomerulus.

Lipofuscin

Lipofuscin is an intracellular, age-related, fluorescent, cytoplasmic, granular pigment found mainly in secondary lysosomes of postmitotic cells [40]. We assessed lipofuscin in proximal, nonproximal, and atrophic tubules for four different areas in the kidney: superficial cortex, mid-cortex, juxtamedullary cortex, and medulla. Lipofuscin was usually absent at 1 month: only one of the six 1-month-old rats displayed any lipofuscin, confined to occasional tubules of the juxtamedullary cortex and medulla. Lipofuscin was present in every kidney of the 9-month-old and 24-month-old animals (Table 3), confined to tubular cells, mainly proximal tubules. Highest amounts were found in atrophic tubular cells. Thus like SA-β-GAL lipofuscin increased in growth and in aging.

Lipofuscin appeared in proximal tubules in all four areas of the 9-month-old group, whereas nonproximal tubules were only affected in one out of six rats. The 24-month-old kidneys displayed a further increase in lipofuscin in proximal tubules in all areas and in nonproximal tubules in superficial and mid cortex. Lipofuscin was present in up to 50% of atrophic tubules in the 24-month-old kidneys.

In both the 9-month-old and the 24-month-old kidneys lipofuscin was significantly associated with SA-β-GAL staining (Table 4).

DISCUSSION

To explore the relationship between cellular senescence and the phenotypic changes of aging, we studied whether features that characterize senescent cells in vitro can be detected in vivo in a well-studied model of renal aging, the Fischer 344 rat kidney. We found that rat kidneys had long telomeres that did not shorten with age, unlike telomeres in human renal cortex, which were much shorter and shortened further with age [36]. The cyclin-dependent kinase inhibitor p16^{INK4a}, a marker of senescence for murine and human cells in culture [16, 17, 41], increased strikingly both with growth and aging and emerges as a unique marker for somatic cell senescence in growth and aging in the kidney. Lipofuscin and SA-β-GAL staining, markers of senescence in vitro, increased in tubular epithelium with age, with lipofuscin appearing first in the medulla and juxtamedullary cortex. Thus in rat kidney, the epithelial cells manifest cell senescence changes independent of telomere shortening, which may contribute to the renal aging phenotype. Since these changes in culture are indicative of environmental stress, our findings indicate that renal senescence in the rat is caused at least in part by environmental stress-induced cellular changes similar to those in senescent cells in vitro, but that telomere attrition does not play a role.

The long telomeres that failed to shorten with age in rat kidneys are consistent with the recent realization that mouse cells in culture have long telomeres that do not shorten with cycling [11]. However, this is the first demonstration of this principle in vivo. In culture, mouse cells do not use telomere shortening as a cell cycle counting mechanism, but nevertheless still reach senescence after fewer cycles than human cells [11, 12, 42]. Thus, rodent cells are much more sensitive to environmental stress than human cells in vitro and possibly in vivo [42]. Mouse fibroblasts rely more on the p53 pathway to limit their proliferative capacity in vitro, and inactivation of p53

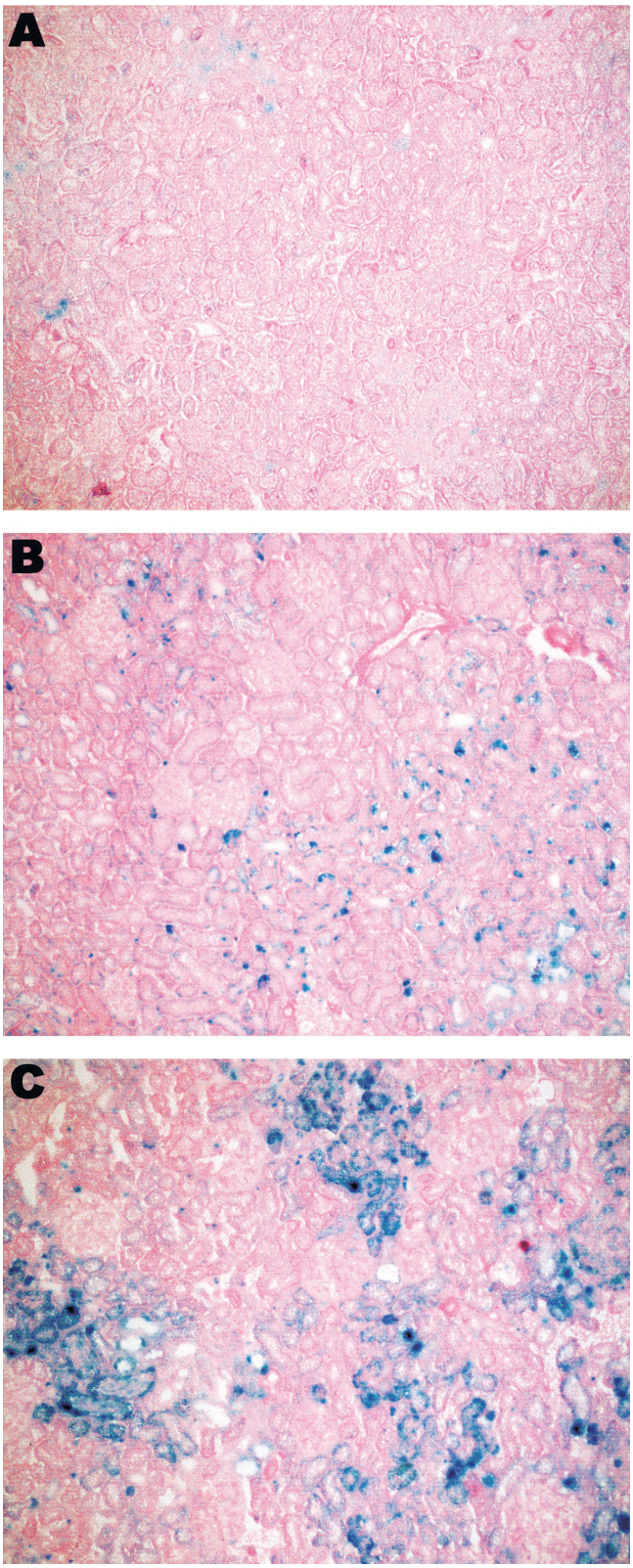

Fig. 5. Representative SA-β-GAL staining in rat kidney tissue from a 1-month-old (*A*), 9-month-old (*B*), 24-month-old rat (*C*). Frozen sections were fixed with 2% formaldehyde/0.2% glutaraldehyde and incubated for 14 hours at 37°C with SA-β-GAL staining solution. Counterstaining was performed with eosin. SA-β-GAL staining was only found in tubules. Glomeruli and vessels were not affected. SA-β-GAL staining was rarely found in kidneys from 1-month-old rats. Increased staining was found in 9-month-old kidneys, and 24-month-old specimens showed a patchy pattern of intense staining.

Table 3. Lipofuscin distribution (%) in tubular epithelium of rat kidney

	M ± SD		
Groups	1 month	9 months	24 months
Superficial cortex			
Proximal tubules	0	0.6 ± 0.8[a]	5.6 ± 3.3[b]
Nonproximal tubules	0	0	0.6 ± 0.5[b]
Atrophic tubules	—	—	29.3 ± 15.9
(atrophic tubules [%])	N/A	N/A	2.0
Mid cortex			
Proximal tubules	0	2.2 ± 1.1[a]	8.7 ± 5.2
Nonproximal tubules	0	0	0.8 ± 0.8[b]
Atrophic tubules	—	—	24.3 ± 14.1
(atrophic tubules [%])	N/A	N/A	2.3
Juxtamedullary cortex			
Proximal tubules	0.04 ± 0.1	3.3 ± 1.5[a]	10.8 ± 5.8[b]
Nonproximal tubules	0	0.2 ± 0.4	0.6 ± 0.8
Atrophic tubules	—	—	33.2 ± 13.8
(atrophic tubules [%])	N/A	N/A	3.4
Medulla			
Proximal tubules	0.1 ± 0.3	5.8 ± 1.9[a]	13.7 ± 10.1
Nonproximal tubules	0	0.1 ± 0.3	0.8 ± 0.8
Atrophic tubules	—	—	49.8 ± 9.0
(atrophic tubules [%])	N/A	N/A	2.3
Total			
Proximal tubules	0.04 ± 0.1	3.3 ± 0.7	10.0 ± 6.0[b]
Nonproximal tubules	0	0.1 ± 0.1	0.7 ± 0.3[b]
Atrophic tubules	—	—	43.9 ± 11.0
(atrophic tubules [%])	N/A	N/A	1.4

[a] 1-month-old and 9-month-old group differ $P < 0.05$
[b] 9-month-old and 24-month-old group differ $P < 0.05$

Table 4. Association of lipofuscin with SA-β-GAL staining in tubular epithelium

Tubules with lipofuscin	SA-β-GAL staining positive	SA-β-GAL staining negative	*P* value[a]
9-month-old rats	73.7%	26.3%	<0.001
24-month-old rats	70.0%	30.0%	<0.001

[a] 2 × 2 table with Yates correction

and/or retinoblastoma/p16^{INK4a} are sufficient to bypass senescence [43–45]. In human cells, inactivation of these pathways prolongs the lifespan of the cell but does not lead to immortalization because the telomere replication counter is operative. These differences may reflect the necessity for long-lived species to have better protection against environmental stress and oncogenesis.

Our findings are compatible with a role for p16^{INK4a} in the cell senescence phenotype in vivo in rat kidney. In mouse fibroblasts in vitro, p16^{INK4a} is strongly associated with senescence, and may specifically reflect cumulative injury from environmental stress. In the present studies,

specimens from kidney, brain, heart, and spleen showed a striking increase in $p16^{INK4a}$ with age. Interestingly, all rats tested showed some $p16^{INK4a}$ expression in heart and spleen at 1 month of age, whereas no expression was found in 10 out of 11 kidneys or in brain. The increase in $p16^{INK4a}$ in brain was found between 1 and 9 months during the growth and development period. For kidney, however, $p16^{INK4a}$ increased in the growth-related and the aging-related phase.

Lipofuscin and SA-β-GAL, which are characteristic of senescent cells, are a manifestation of age-induced cellular deterioration and could cause in some aspects of the phenotype of aging. Lipofuscin accumulated in proximal tubules and particularly in atrophic tubules, suggesting that these segments manifest more age-related stress and that the tubules with lipofuscin are prone to atrophy. Alternatively the lipofuscin in atrophic tubules may be a reflection of atrophy, rather than a cause. Staining for SA-β-GAL was significantly associated with lipofuscin, but more tubules displayed SA-β-GAL than lipofuscin, suggesting that staining for SA-β-GAL could be an earlier or more prevalent manifestation of senescence. Lipofuscin accumulates with age in many organs, most strikingly in heart and brain. Lipofuscin is derived from oxidized proteins and lipids and forms in secondary lysosomes due their nondegradability [40]. SA-β-GAL activity has been attributed to a rise in the level of the lysosomal form of this enzyme [46, 47], as a consequence of an increase in lysosomal mass in senescent cells [47, 48]. Lipofuscin and SA-β-GAL may thus both be independent manifestations of impaired homeostasis of cell organelles with age, with SA-β-GAL being an earlier or more widespread marker than lipofuscin.

While distinguishing age-related disease from aging is difficult and often becomes a semantic argument, we believe that the molecular changes described here are related to cumulative effects of environmental stress during growth, development, and aging, and not due to disease. Our rats showed changes typical of aging in all rat strains, although milder than often described. Some rats have a high frequency of apparent age-related renal changes, which can vary with the environmental condition [33]. However, in our 24-month-old rats only 4.4% of glomeruli showed signs of sclerosis and the percentage of atrophic tubules did not exceed 3.4%. Partial segmental sclerosis occurred in 2% of glomeruli. We are aware that the measurement of creatinine, which is a composite of renal function and muscle mass, is not always a reliable indicator for renal function, especially in the elderly when muscle mass is reduced. However, muscle mass remains stable in Fischer 344 rats until the age of 27 months [49]. Glomerular filtration rates in Fischer 344 rats have been previously reported to be stable with age, despite some glomeruli showing spontaneous focal glomerulosclerosis [50, 51] Fischer 344 rats do not develop hypertension [52, 53]. Based on the literature, our histopathologic assessment and the stable creatinine levels, we believe that our old Fischer 344 rats had stable glomerular filtration rates.

The increase in kidney weight in old rats probably reflects the net balance of a complex mixture of hypertrophy, growth, fibrosis, atrophy, and apoptosis. The constant protein/DNA ratio argues against pure hypertrophy. However, the number of tubular cells per tubular cross-section did not increase with age, arguing against pure hyperplasia. Fibrosis that was threefold higher in old than in young rats could contribute to the renal weight increase. An additional factor could be increased water content of older kidneys as reported earlier [51], although we found no overt edema on histopathology. This increase in weight occurs despite an increase in the number of apoptotic cells. Together, these findings suggest that the renal aging phenotype is heterogeneous, which is a general characteristic of aging systems.

We propose that renal aging in rats reflects the cumulative effects of environmental stress, leading to cell cycle arrest similar to mouse fibroblasts in culture despite their long telomeres. The changes of aging are already present in rat kidneys by 9 months, and progress considerably over the next 15 months: SA-β-GAL, lipofuscin, and $p16^{INK4a}$, and the morphologic changes. Our studies indicate that the tubular epithelium deteriorates as key cells needed to replace damaged cells develop organelle and other changes. At one level homeostasis is maintained. Organ mass and function are preserved. Nevertheless, at another level homeostasis is not capable of replacing the cells damaged by presumably oxidant-related stress. Thus accumulation of senescent cells may reflect both environmental stress and limited replacement. The appearance and persistence of damaged cells then compromises homeostatic mechanisms, leading to age-related pathology. Although kidney mass and function can be maintained because of high replicative potential of the nonsenescent cells, the accumulation of the senescent cells reaches critical limits in some nephrons, triggering nephron shutdown by a regulatory mechanism.

ACKNOWLEDGMENTS

The authors are grateful to Dr. Kim Solez for helpful discussions regarding the pathological features in the Fischer 344 rats, to Dr. Alan Thomson for generously providing the rats, and to Dr. Hans Dieter Volk for the TGF-β1 primer/probe sequences. We also wish to thank Gian Jhangri for his help with the statistical analysis and Enid Pehowich and Robin Stocks for technical assistance. This research has been supported by operating grants from the Roche Organ Transplant Research Foundation, the Canadian Institutes of Health Research, the Kidney Foundation of Canada, Novartis Pharmaceuticals Canada, Inc., The Muttart Foundation, and The Royal Canadian Legion. Dr. Philip Halloran holds a Canada Research Chair in Life Sciences Related to Human Health and Disease.

Reprint requests to Anette Melk, M.D., Division of Nephrology & Immunology, University of Alberta, 250 Heritage Medical Research Centre, Edmonton, Alberta T6G 2S2 Canada.
E-mail: anettemelk@yahoo.de

REFERENCES

1. Levi M, Rowe JW: Aging and the kidney, chap. 88, in *Diseases of the Kidney, 5 ed*., edited by Schrier RW, Gottschalk CW, Boston, MA, Little, Brown, and Company, 1993, pp 2405–2432
2. Pannu N, Halloran PF: The kidney in aging, chap. 57, in *Primer on Kidney Diseases, 3 ed.*, edited by Greenberg A, San Diego, CA, Academic Press, 2001, pp 377–381
3. Epstein M: Aging and the kidney. *J Am Soc Nephrol* 7:1106–1122, 1996
4. Lindeman RD, Goldman R: Anatomic and physiologic age changes in the kidney. *Exp Geront* 21:379–406, 1986
5. Gourtsoyiannis N, Prassopoulos P, Cavouras D, Pantelidis N: The thickness of the renal parenchyma decreases with age. A CT study of 360 patients. *Am J Roentgenol* 155:541–544, 1990
6. Filser D, Zeier M, Nowack R, Ritz E: Renal functional reserve in healthy elderly subjects. *J Am Soc Nephrol* 3:1371–1377, 1993
7. Nyengaard JR, Bendtsen TF: Glomerular number and size in relation to age, kidney weight, and body surface in normal man. *Anat Rec* 232:194–201, 1992
8. Johnson FB, Sinclair DA, Guarente L: Molecular biology of aging. *Cell* 96:291–302, 1999
9. Finch CE, Tanzi RE: Genetics of aging. *Science* 278:407–411, 1997
10. Hayflick L, Moorhead PS: The serial cultivation of human diploid cell strains. *Exp Cell Res* 25:585–621, 1961
11. Wright WE, Shay JW: Telomere dynamics in cancer progression and prevention: Fundamental differences in human and mouse telomere biology. *Nat Med* 6:849–851, 2000
12. Blasco MA, Lee H-W, Hande MP, *et al*: Telomere shortening and tumor formation by mouse cells lacking telomerase RNA. *Cell* 91:25–34, 1997
13. Lee H-W, Blasco MA, Gottlieb GJ, *et al*: Essential role of mouse telomerase in highly proliferative organs. *Nature* 392:569–574, 1998
14. Tang DG, Tokumoto YM, Apperly JA, *et al*: Lack of replicative senescence in cultured rat oligodendrocyte precursor cells. *Science* 291:868–871, 2001
15. Mathon NF, Malcolm DS, Harrisingh MC, *et al*: Lack of replicative senescence in normal rodent glia. *Science* 291:872–875, 2001
16. Serrano M, Lee H-W, Chin L, *et al*: Role of the INK4a locus in tumor suppressor and cell mortality. *Cell* 85:27–37, 1996
17. Zindy F, Quelle DE, Roussel MF, Sherr CJ: Expression of the $p16^{INK4a}$ tumor suppressor versus other INK4 family members during mouse development and aging. *Oncogene* 15:203–211, 1997
18. Sharpless NE, Bardeesy N, Lee KH, *et al*: Loss of $p16^{Ink4a}$ with retention of $p19^{Arf}$ predisposes mice to tumorigenesis. *Nature* 413:86–91, 2001
19. Krimpenfort P, Quon KC, Mooi WJ, *et al*: Loss of $p16^{Ink4a}$ confers susceptibility to metastatic melanoma in mice. *Nature* 413:83–86, 2001
20. Baylis C, Corman B: The aging kidney: Insights from experimental studies. *J Am Soc Nephrol* 9:699–709, 1998
21. Corman B, Pratz J, Poujeol P: Changes in anatomy, glomerular filtration, and solute excretion in aging rat kidney. *Am J Physiol* 248:R282–R287, 1985
22. Dodane V, Chevalier J, Bariety J, *et al*: Longitudinal study of solute excretion and glomerular ultrastructure in an experimental model of aging rats free of kidney disease. *Lab Invest* 64:377–391, 1991
23. Bich-Thuy L, Fauci AS: Recombinant interleukin-2 and gamma-interferon (IFN-γ) act synergistically on distinct steps of in vitro terminal human B cell maturation. *J Clin Invest* 77:1173–1179, 1986
24. Mather MW: Base composition-independent hybridization in dried agarose gels: Screening and recovery for cloning of genomic DNA fragments. *Biotechniques* 6:444–447, 1988
25. Harley CB, Futcher AB, Greider CW: Telomeres shorten during ageing of human fibroblasts. *Nature* 345:458–460, 1990
26. Chirgwin JM, Pryzybyla AE, MacDonald RJ, Rutter WJ: Isolation of biologically active ribonucleic acid from sources enriched in ribonuclease. *Biochemistry* 18:5294–5299, 1979
27. Heid CA, Stevens J, Livak KJ, Williams PM: Real time quantitative PCR. *Genome Res* 6:986–994, 1996
28. Dimri GP, Lee X, Basile G, *et al*: A biomarker that identifies senescent human cells in culture and in aging skin in vivo. *Proc Natl Acad Sci USA* 92:9363–9367, 1995
29. Chkhotua A, Shapira Z, Tovar A, *et al*: Cellular senescence: A new marker of kidney function recovery after ischemic injury in rats. *Transplant Proc* 33:2910–2915, 2001
30. Coleman GL, Barthold W, Osbaldiston GW, *et al*: Pathological changes during aging in barrier-reared Fischer 344 male rats. *J Gerontol* 32:258–278, 1977
31. Maeda H, Gleiser CA, Masoro EJ, *et al*: Nutritional influences on aging of Fischer 344 rats. *II. Pathol J Gerontol* 40:671–688, 1985
32. Yu BP, Masoro EJ, McMahan CA: Nutritional influences on aging of Fischer 344 rats: I. Physical, metabolic, and longevity characteristics. *J Gerontol* 40:657–670, 1985
33. Masoro EJ: Mortality and growth characteristics of rat strains commonly used in aging research. *Exp Aging Res* 6:219–233, 1980
34. Racusen LC, Solez K, Colvin RB, *et al*: The Banff 97 working classification of renal allograft pathology. *Kidney Int* 55:713–723, 1999
35. Starling JA, Maule J, Hastie ND, Allshire RC: Extensive telomere repeat arrays in mouse are hypervariable. *Nucleic Acids Res* 18:6881–6888, 1990
36. Melk A, Ramassar V, Helms LM, *et al*: Telomere shortening in kidneys with age. *J Am Soc Nephrol* 11:444–453, 2000
37. Bodnar AG, Ouellette M, Frolkis M, *et al*: Extension of life-span by introduction of telomerase into normal human cells. *Science* 279:349–352, 1998
38. Sigal SH, Rajvanshi P, Gorla GR, *et al*: Partial hepatectomy-induced polyploidy attenuates hepatocyte replication and activates cell aging events. *Am J Physiol* 276:G1260–G1272, 1999
39. Ding G, Franki N, Kapasi AA, *et al*: Tubular cell senescence and expression of TGF-beta1 and p21(WAF1/CIP1) in tubulointerstitial fibrosis of aging rats. *Exp Mol Pathol* 70:43–53, 2001
40. Terman A, Brunk UT: Lipofuscin: Mechanisms of formation and increase with age. *APMIS* 106:265–276, 1998
41. Palmero I, McConnell B, Parry D, *et al*: Accumulation of $p16^{INK4a}$ in mouse fibroblasts as a function of replicative senescence and not of retinoblastoma gene status. *Oncogene* 15:495–503, 1997
42. Sherr CJ, DePinho RA: Cellular senescence: mitotic clock or culture shock? *Cell* 102:407–410, 2000
43. Kamijo T, Zindy F, Roussel MF, *et al*: Tumor suppression at the mouse *INK4a* locus mediated by the alternative reading frame product $p19^{ARF}$. *Cell* 91:649–659, 1997
44. Harvey M, Sands AT, Weiss RS, *et al*: In vitro growth characteristics of embryo fibroblasts isolated from p53-deficient mice. *Oncogene* 8:2457–2467, 1993
45. Harvey DM, Levine AJ: p53 alteration is a common event in the spontaneous immortalization of primary BALB/c murine embryo fibroblasts. *Genes Dev* 5:2375–2385, 1991
46. Krishna DR, Sperker B, Fritz P, Klotz U: Does pH 6 beta-galactosidase activity indicate cell senescence? *Mech Ageing Dev* 109:113–123, 1999
47. Kurz DJ, Decary S, Hong Y, Erusalimsky JD: Senescence-associated (beta)-galactosidase reflects an increase in lysosomal mass during replicative ageing of human endothelial cells. *J Cell Sci* 113 (Pt 20):3613–3622, 2000
48. Robbins E, Levine EM, Eagle H: Morpholigic changes accompanying senescence of cultured human diploid cells. *J Exp Med* 131: 1211–1222, 1970
49. Yu BP, Masoro EJ, Murata I, *et al*: Life span study of SPF Fischer 344 male rats fed ad libitum or restricted diets: Longevity, growth, lean body mass and disease. *J Gerontol* 37:130–141, 1982
50. Van Liew JB, Davis FB, Davis PJ, *et al*: Calorie restriction decreases microalbuminuria associated with aging in barrier-raised Fischer 344 rats. *Am J Physiol* 263:F554–F561, 1992
51. Bengele HH, Mathias RS, Perkins JH, Alexander EA: Urinary concentrating defect in the aged rat. *Am J Physiol* 240:F147–F150, 1981
52. Kregel KC, Johnson DG, Tipton CM, Seals DR: Cardiovascular-sympathetic adjustments to nonexertional heat stress in mature and senescent Fischer 344 rats. *J Appl Physiol* 69:2043–2049, 1990
53. Herlihy JT, Kim S-W: Modulation of the aging cardiovascular system by dietary restriction, chap. 3, in *Modulation of Aging Processes by Dietary Restriction,* edited by Yu BP, Boca Raton, CRC Press, 2002, pp 57–87